Investigation of high sensitivity radio-frequency readout circuit based on AlGaN/GaN high electron mobility transistor*

Zhang Xiao-Yu(张晓渝)[a)†], Tan Ren-Bing(谭仁兵)[b)], Sun Jian-Dong(孙建东)[a)],
Li Xin-Xing(李欣幸)[a)], Zhou Yu(周 宇)[a)], Lü Li(吕 利)[a)], and Qin Hua(秦 华)[a)‡]

[a)] *Key Laboratory of Nanodevices and Applications, Suzhou Institute of Nano-tech and Nano-bionics, Chinese Academy of Sciences, Suzhou* 215125, *China*

[b)] *School of Mathematics and Physics, Chongqing University of Science and Technology, Chongqing* 401331, *China*

(Received 10 March 2015; revised manuscript received 17 May 2015; published online 20 August 2015)

An AlGaN/GaN high electron mobility transistor (HEMT) device is prepared by using a semiconductor nanofabrication process. A reflective radio-frequency (RF) readout circuit is designed and the HEMT device is assembled in an RF circuit through a coplanar waveguide transmission line. A gate capacitor of the HEMT and a surface-mounted inductor on the transmission line are formed to generate LC resonance. By tuning the gate voltage V_g, the variations of gate capacitance and conductance of the HEMT are reflected sensitively from the resonance frequency and the magnitude of the RF reflection signal. The aim of the designed RF readout setup is to develop a highly sensitive HEMT-based detector.

Keywords: radio-frequency circuit, high electron mobility transistor

PACS: 52.70.Gw, 85.30.–z, 73.61.Ey **DOI:** 10.1088/1674-1056/24/10/105201

1. Introduction

The GaN high-electron mobility transistor (HEMT) has great potential applications in high frequency and high power electronic devices.[1–3] With the development of GaN transistor technology, the GaN HEMT has demonstrated its high power density and high efficiency over the Si- and GaAs-based radio-frequency (RF) and microwave transistors.[4,5] Thus, for the same output power, the reduction in device size can be realized using GaN-based devices in place of conventional devices. AlGaN/GaN heterostructure has the advantages of the discontinuity of conduction band ΔE and large polarization efficient in nitride, which results in a large piezoelectric polarization in the epitaxial layer of GaN.[6–8] The high concentration of two-dimensional electron gas (2DEG) is observed at the interface of AlGaN/GaN heterostructure. Therefore, AlGaN/GaN HEMT is an important tunable material for RF and microwave devices by controlling the concentration of 2DEG under gate voltage (V_g). The RF readout circuit, invented by Schoelkopf *et al.*[9] in 1998, is used to investigate the RF single-electron transistor for the most sensitive and fastest electrometer.[10] The device, such as the single-electron transistor or quantum point contact based on Si or AlGaAs/GaAs heterostructure, is embedded in an RF transmission line of the readout circuit. The changed properties of the device are reflected sensitively from the RF output signal. In China, the use of RF readout to investigate the device has been studied only a very little. In the present paper, we develop a reflective RF readout circuit in which a tunable AlGaN/GaN HEMT device is assembled in the circuit to investigate the performance of the RF readout setup. Under the applied V_g, the changes of impedance including gate capacitance and source–drain conductance are reflected sensitively to the RF output signal. The sensitive changes in resonant frequency and magnitude of output signal indicate that the RF readout setup can be applied to the high-speed detector for the applications in electromagnetic or optoelectronic devices.[11]

2. Experiments

The $Al_{0.3}Ga_{0.7}N$/GaN heterostructure provided a 2DEG about 25 nm below the surface. The electron mobility μ and density n_s at 300 K were $\mu = 1950$ cm^2/V·s and $n_s = 1.4 \times 10^{13}$ cm^{-2}, respectively, which were determined by Hall measurement.[12] Ultra-violet exposure, lithography, lift-off, Ohmic electrode preparation, and ion beam etching techniques were used to fabricate the HEMT microstructures. The gate length of HEMT was $l = 2$ μm and the channel (mesa) width was $w = 8$ μm. A thin film of 10-nm Al_2O_3 was deposited as the insulating layer by atomic layer deposition. The top electrode of the Ni/Au layer with 200 nm was fabricated by using electron beam evaporation. The microstructure of HEMT was

*Project supported by the National Natural Science Foundation of China (Grant No. 61107093), the Suzhou Science and Technology Project, China (Grant No. ZXG2012024), and the Youth Innovation Promotion Association, Chinese Academy of Sciences (Grant No. 2012243).

†Corresponding author. E-mail: xyzhang2010@sinano.ac.cn

‡Corresponding author. E-mail: hqin2007@sinano.ac.cn

© 2015 Chinese Physical Society and IOP Publishing Ltd

characterized by using scanning electron microscopy (SEM).

The radio frequency (RF) readout setup mainly included a voltage-controlled oscillator (VCO), directional coupler, low noise amplifier (LNA), band-pass filter (BPF), DC block, and RF detector (Agilent 8471D). The output power from VCO (0.4 GHz–1.3 GHz) was about +8 dBm. HEMT and high-Q inductors ($L = 100$ nH) were surface mounted on the 50-Ω coplanar waveguide transmission line, which is fabricated on a high-frequency printed-circuit board (Rogers 3010). The HEMT device was electrically connected to the PCB by using short gold bond wires. The mounted inductor (L) and the capacitance (C) of HEMT formed an LC resonant unit. The LC circuit introduced a discontinuity in the electromagnetic impedance in the transmission line which reflected an incident RF signal. All RF components and transmission lines were connected by soft coaxial cables. The gate voltage V_g was supplied by a Yokogawa DC source meter.

3. Experiments and discussion

Figure 1 shows the schematic diagram of the RF readout circuit. The incoming RF signal from the VCO is coupled to the HEMT device by a directional coupler and the reflected RF signal passes through the directional coupler to LNA, BPF, and DC block to the RF detector. The RF detector is used in RF circuits as a detecting element in the leveling loop for power monitoring. Finally, the reflected RF signal can be monitored by a multimeter. The inset shows the image of the transmission line where the HEMT device and high-Q inductors are surface mounted. The device on the copper holder must be well grounded in order to avoid damaging the HEMT device by static electricity. An SEM photo of the HEMT is also shown in the inset where mesa and Ohmic electrodes are displayed.

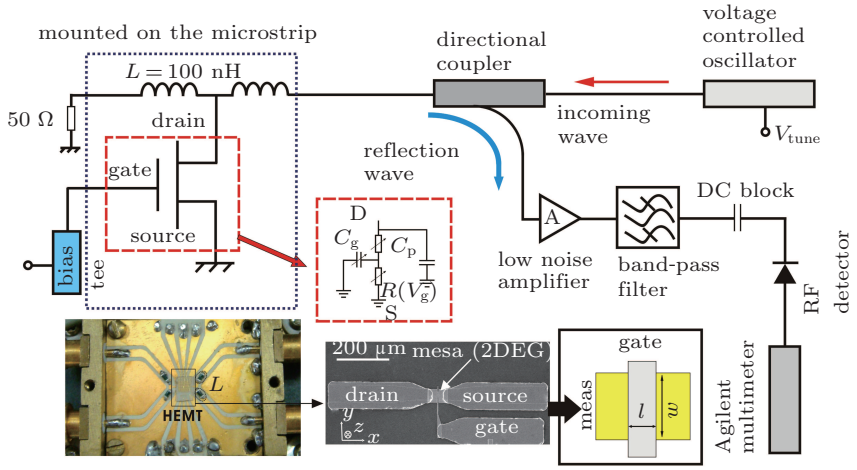


Fig. 1. (color online) Schematic diagram of the RF readout circuit and equivalent circuit of HEMT. Inset shows the image of the transmission line with the HEMT device and SEM photo of HEMT.

Figure 2 shows the variations of the transfer characteristic curve of AlGaN/GaN HEMT, i.e., drain–source DC current I_{ds} with gate voltage V_g. For I_{ds}–V_g measurement, a DC voltage V_{ds} is applied to the drain and V_g is applied to the gate. A multimeter through a low-noise current preamplifier with a sensitivity of 10^{-4} A/V is used to monitor the I_{ds} at source. At a fixed V_{ds}, I_{ds} decreases with the increase of $|V_g|$ and reaches a saturation state when $V_g < -3.75$ V, showing a switch characteristic of depleting the electrons under the control of V_g. The current I_{ds} can be described as follows:

$$I_{ds} = \mu C_g(V_g)\frac{w}{l}[(V_g - V_{th})V_{ds} - \tfrac{1}{2}V_{ds}^2], \quad (1)$$

where μ is the electron mobility, C_g is the gate capacitance, and V_{th} is a threshold voltage where I_{ds} changes abruptly. Generally, equation (1) is used to describe the I_{ds} under the gate and it is difficult to fit the whole I_{ds}–V_g curve because the C_g is also a function of V_g. When V_g is zero, I_{ds} increases greatly with the increase of V_{ds} because the electrons in the channel of the HEMT are accelerated by V_{ds}, thus resulting in the enhancement of the drift current.

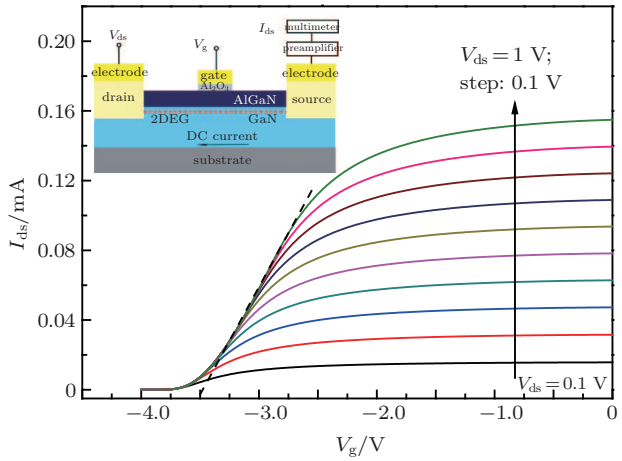


Fig. 2. (color online) Curves of I_{ds} versus V_g at different values of applied V_{ds}. Inset shows the schematic diagram of GaN/AlGaN HEMT.

Figure 3 shows the variations of the RF reflection signal V_{RF} with frequency. Two remarkable characteristics are observed. Firstly, the resonance frequency f_r shifts from 805 MHz to 816 MHz with the increase of $|V_g|$. Secondly, it is found that the magnitude of RF signal V_{RF} also decreases significantly around the resonance frequency with the increase of applied V_g. We consider that the changes of f_r and the magnitude of V_{RF} are strongly dependent on the impedance of HEMT under V_g, namely, the changes of gate capacitance and conductance. In an HEMT microstructure, we estimate the geometry capacitance under the gate to be $C_{geom} = wl\varepsilon_0\varepsilon_{AlGaN}/d_{AlGaN} = 0.053$ pF, where $wl = 16$ μm^2 is the area under the gate, ε_0 is the vacuum permittivity, $\varepsilon_{AlGaN} = 9.4$ is the relative permittivity of AlGaN, and $d_{AlGaN} = 25$ nm is the distance between the gate and 2DEG. With the increase of V_g, the electrons under the gate are gradually depleted, thus resulting in the change of electric charges Δq in the GaN layer. The reduced electron density in 2DEG can be equivalent to the increase of distance d_{AlGaN}, therefore, the gate capacitance decreases with the applied V_g.[13,14] According to the resonance of the designed LC circuit, the resonance frequency is expressed as

$$f_r = \frac{1}{2\pi\sqrt{LC_{RF}/2}}, \tag{2}$$

which is mainly dominated by the capacitance C_{RF} including gate capacitance and parasitic capacitance, when $L = 100$ nH is a constant in our experiment. Therefore, f_r increases with the decrease of C_{RF} under V_g, which is consistent with the observed shift of f_r in Fig. 3. On the other hand, the source–drain resistance R_{ds} will also increase with the applied V_g increasing due to the depletion of electrons. It is suggested that the variation of the magnitude of reflection signal V_{RF} originates from the change of source–drain conductance.

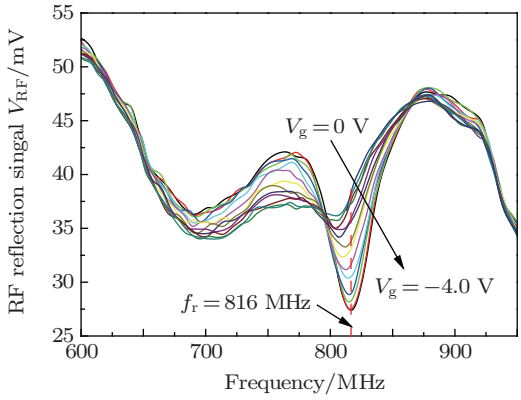


Fig. 3. (color online) Variations of reflected voltage signal with frequency at different values of applied V_g.

Figure 4(a) shows the calculated capacitance C_{RF} as a function of V_g from Eq. (2) by using the measured f_r where the value of the inductor is $L = 100$ nH. Clearly, the obtained C_{RF} displays the V_g-controlled characteristics, which indicates that the changed capacitance of the HEMT is reflected sensitively at V_{th} by the RF readout circuit. We observe that C_{RF} varies from 0.378 pF to 0.366 pF when the value of V_g changes from 0 V to −4 V. The tunability $\tau = [C_{RF}(V_g = 0)–C_{RF}(V_g = -4\text{ V})]/C_{RF}$ $(V_g = 0)$ is about 3.2% around the frequency of 816 MHz. Actually, the tunability of gate capacitance is remarkable from the measurement of the gate capacitance C_{meas} at a low frequency of 1 kHz by using an Agilent B1500A semiconductor device analyzer as shown in Fig. 4(b). The V_g-controlled C_{meas} varies from 0.25 pF to 0.042 pF, and the tunability reaches up to 83.2%, showing a good V_g-controlled performance at the low frequency. We consider that the difference in tunability mainly results from the difference in frequency response of gate capacitance.

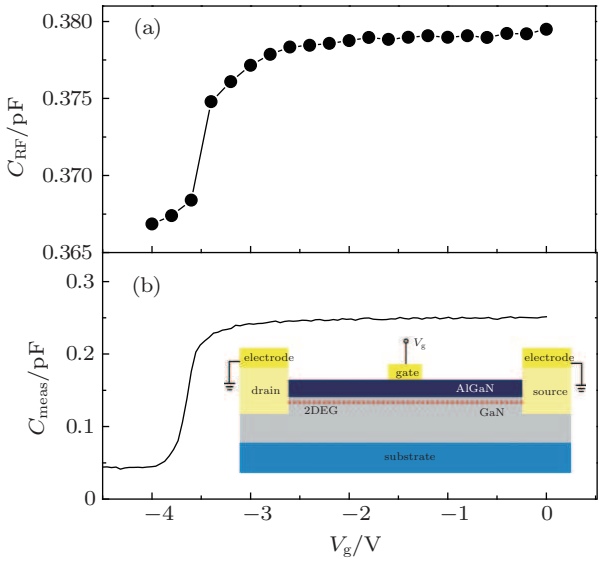


Fig. 4. (color online) Variations of (a) calculated capacitance and (b) measured capacitance with V_g at 1 kHz.

Figure 5 shows the variations of source–drain conductance $G(1/R_{ds})$ and the valley of RF reflection signal V_m in Fig. 3 with V_g. The conductance of HEMT $G = n_s e\mu w/l$ is mainly dependent on the electron density n_s and mobility μ when the micro-structure of HEMT is fixed. With the increase of applied V_g, conductance G decreases abruptly in the vicinity of V_{th} due to the depletion of electrons. We find that the V_m also exhibits the same variation trend as the G–V_g relationship. From the RF equivalent circuit in our previous article,[10] the reflection coefficient is $\Gamma = (Z_{in} - Z_0)/(Z_{in} + Z_0)$, where Z_{in} is the input impedance and $Z_0 = 50$ Ω is a characteristic impedance. The input impedance can be expressed as $Z_{in} = j2\pi fL + R_{ds}/[1 + j2\pi fR_{ds}C] + Z_0$. In the experiment, capacitance C mainly includes gate capacitance C_g and the parasitic capacitance of the circuit. The sensitivity of the

output signal under the gate voltage is proportional to both $\mathrm{d}(1-\Gamma)/\mathrm{d}R_{\mathrm{ds}}(V_{\mathrm{g}})$ and $\mathrm{d}R_{\mathrm{ds}}(V_{\mathrm{g}})/\mathrm{d}V_{\mathrm{g}}$. The first term is determined by the characteristics of the RF transmission line, while the second term is determined by the characteristic of the HEMT. The intrinsic sensitivity $|\mathrm{d}R_{\mathrm{ds}}/\mathrm{d}V_{\mathrm{g}}|$ of the readout circuit is strongly dependent on the rate of changed drain–source resistance $R_{\mathrm{ds}}(V_{\mathrm{g}})$. Therefore, the design and fabrication of good performance of HEMT with large $|\mathrm{d}R_{\mathrm{ds}}/\mathrm{d}V_{\mathrm{g}}|$ are the key to improving the sensitivity of the readout setup, namely, the rapid change of source–drain resistance near threshold voltage V_{th} under V_{g}. In the present experiment, the sensitivity of the readout setup can increase up to 5.6×10^{8}. When a threshold voltage V_{th} is applied to the gate of the HEMT, the RF readout setup can be used to detect sensitively the change of impedance of HEMT under the external radiation, such as terahertz radiation or light.

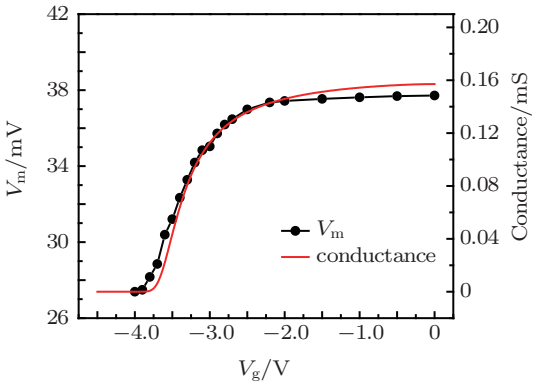


Fig. 5. (color online) Variations of the valley of RF reflection signal V_{m} and conductance with V_{g}.

4. Conclusions

We designed a reflective RF readout circuit and investigated the performance of the HEMT-based readout setup. The RF setup is used to detect the changed impedance of the HEMT by analyzing the resonance frequency and the magnitude of the RF reflection signal. It is suggested that the designed RF readout setup can be applied to the readout circuit for high-sensitivity optic–electric detection.

References

[1] Mishra U K, Parikh P and Wu Y F 2002 *Proc. IEEE* **90** 1022
[2] Chen Q, Yang J W, Gaska R and Asif Khan M 1998 *IEEE Electron Dev. Lett.* **19** 44
[3] Mishra U K, Wu Y F, Keller B P, Keller S and Denbaars S P 1998 *IEEE Trans. Microwave Theor. Technol.* **46** 756
[4] Wu Y F, Kapolnek D, Ibbetson J P, Parikh P, Keller B P and Mishra U K 2001 *IEEE Trans. Electron Dev.* **48** 586
[5] Sheppard S T, Doverspike K, Pribble W L, Allen S T and Palmour J W 1999 *IEEE Electron Dev. Lett.* **20** 161
[6] Lei Z F, Guo H X, Zeng C, Chen H, Wang Y S and Zhang Z G 2015 *Chin. Phys. B* **24** 056103
[7] Zhang P, Zhao S L, Hou B, Wang C, Zheng X F, Ma X H, Zhang J C and Hao Y 2015 *Chin. Phys. B* **24** 037304
[8] Sun Y F, Sun J D, Zhang X Y, Qin H, Zhang B S and Wu D M 2012 *Chin. Phys. B* **21** 108504
[9] Schoelkopf R J, Wahlgren P, Kozhevnikov A A, Delsing P and Prober D E 1998 *Science* **280** 1238
[10] Qin H and Williams D A 2006 *Appl. Phys. Lett.* **88** 203506
[11] Chen Y, Daigle A, Fitchorov T, Hu B, Geiler M, Geiler A, Vittoria C and Harris V G 2011 *Appl. Phys. Lett.* **98** 202502
[12] Sun J D, Qin H, Lewis R A, Sun Y F, Zhang X Y, Cai Y, Wu D M and Zhang B S 2012 *Appl. Phys. Lett.* **100** 173513
[13] Maeda N, Nishida T, Kobayashi N and Tomizawa M 1998 *Appl. Phys. Lett.* **73** 1856
[14] Ambacher O, Foutz B, Smart J, Shealy J R, Weimann N G, *et al.* 2000 *J. Appl. Phys.* **87** 334